Journal of The Physical Society of Japan
Vol. 60, No. 9, September, 1991, pp. 3032–3044

Intra- and Intermolecular Correlations in Liquid Selenium-Halogen Systems

Kenji MARUYAMA, Yukinobu KAWAKITA, Makoto YAO, Hirohisa ENDO and Masakatsu MISAWA†

Department of Physics, Faculty of Science, Kyoto University, Kyoto 606
†*National Laboratory for High Energy Physics, Tukuba 305*

(Received May 13, 1991)

The structure of liquid (l-) selenium-halogen mixtures has been studied by both EXAFS and neutron scattering measurements. The concentration variation of the coordination numbers of Se and halogen atoms around the central Se atom were determined. It was found that all Cl atoms in l-$Se_{1-x}Cl_x$ act as chain terminators. The rapid contraction of Se–Se and Se–Cl bonds was observed when the Cl concentration approached 0.5. For l-$Se_{1-x}I_x$, I atoms are not always incorporated into the chain molecules, and the excess I atoms form I_2 molecules. The intermolecular orientational correlation for l-$Se_{0.5}Cl_{0.5}$ and l-$Se_{0.5}Br_{0.5}$ will be discussed utilizing the results of the neutron scattering experiments.

§1. Introduction

The measurements of viscosity,[1] magnetic susceptibility[2–4] and NMR[3,5] have suggested that the Se chain is composed by 10^4 to 10^5 atoms on the average near the melting point and that it becomes shorter as the temperature is raised. When the chain scission occurs in the liquid state, neutral dangling-bond states are created at the chain ends.

The viscosity of liquid Se is decreased substantially by adding halogen impurities.[1,6] Recently we have found that the electrical conductivity increases considerably and the thermopower becomes large and positive when halogen impurities are doped into liquid Se, and that these impurity effects increase with the increasing electronegativity of the halogen atom.[7,8] These results suggest that the impurity may have a strong influence on the modification of the chain structure.

It is interesting that in Se–halogen binary systems the melting point decreases dramatically with increasing halogen concentration, up to the eutectic composition of about 50 at.% halogen.[9–11] In the case of the Se–Cl system the eutectic temperature is as low as about −50°C. It has been reported that there exists a stable crystalline form,[9,12] which consists of Se_2Cl_2 molecules, at 50 at.% Cl, while in the gas phase $SeCl_2$ molecules[13–15] are found to be stable rather than Se_2Cl_2. In the Se–I system,[11] on the other hand, no stable compound has been found in both solid and gas phases. However, no information has been available to-date about the structure of liquid Se-halogen systems.

It has long been argued that EXAFS is a good tool to investigate local structure of disordered systems such as liquids. Nevertheless, there has been little application of the EXAFS technique to liquids. This is largely due to the difficulty of containing a stable liquid sample which is thin enough to transmit the X-ray beam. Recently we have succeeded in overcoming this problem by developing a new sample cell.[16] A more serious problem is the fact that EXAFS signals from a liquid are in general strongly damped, owing to the inherent disorder of the atomic arrangement and thermal agitation.[17] However, the EXAFS signal is unusually large where the photoelectron is backscattered by the covalently bonded neighboring atoms. In addition, EXAFS does not address the low momentum range compared to the X-ray or neutron diffraction method. However, EXAFS can give useful information on the neighboring configuration around a particular atom as long as the atoms are covalently bonded.

Therefore it is expected that intramolecular correlations can be selectively extracted by EXAFS measurements in liquid Se-halogen systems. To determine the spatial correlation beyond the near-neighbor distance, neutron diffraction methods are more useful than EXAFS.

In the present paper we study the intra- and intermolecular correlations in liquid Se-halogen systems by means of EXAFS and neutron diffraction experiments; these methods are complementary in the sense described above.

§2. Experimental

2.1 Sample preparation

Liquid selenium-chlorine mixtures (l-$Se_{1-x}Cl_x$) were prepared by mixing the appropriate masses of granular Se (99.999%) and liquid SeCl (99%) for the concentration range $0<x<0.5$, and by mixing granular Se and $SeCl_4$ powder (99.5%) for $0.5<x<0.8$. The mixtures were sealed in evacuated glass tubes and heated at about 150°C for 1 day. Since $Se_{1-x}Cl_x$ mixtures are easily dissociated into $SeCl_2$ and Cl_2 gases in the presence of moisture, we handled them under dry argon atmosphere.

Liquid $Se_{0.5}Br_{0.5}$ was made from granular Se and $SeBr_4$ powder (99.5%) in a way similar to the $Se_{1-x}Cl_x$ mixtures. We handled the $SeBr_4$ sample in He gas which had been dehydrated by passing it through a liquid nitrogen trap, because $SeBr_4$ is much more sensitive to moisture. Liquid $Se_{1-x}I_x$ mixtures were made from granular Se and I flake (99.8%). The errors in concentration in each case were smaller than 1%.

2.2 EXAFS measurements

Fused quartz was chosen as a sample cell material. (Figure 1 shows this cell.) Two quartz tubes with inner diameters of 4 mm were prepared with closed ends for the X-ray window. These ends were polished to a thickness of about 300 μm in order to improve the efficiency of X-ray transmission. The two tubes were then inserted into an outer tube and welded to it at the ends. The thickness of the sample region was estimated from the thickness of the graphite spacer; this was placed between the two inner tubes before welding and was burned out afterwards.

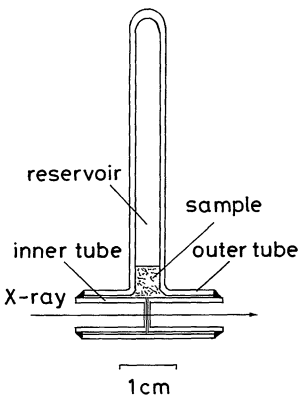

Fig. 1. The quartz cell used for EXAFS measurements on liquid samples.

The sample was sealed in the reservoir of the cell under vacuum and flowed into the test region upon heating. An X-ray photograph confirmed that the test region was completely filled with the liquid sample.

Measurements were taken both in the liquid state and also in the supercooled state, as denoted by the crosses on the phase diagrams[9,11] in Fig. 2. The freezing point was determined by monitoring the density change from the X-ray absorption measurement. The stability of the temperature during a run was better than ±0.5°C.

The EXAFS experiments around the Se K-edge for l-$Se_{1-x}Cl_x$ and l-$Se_{1-x}I_x$ mixtures were carried out using the spectrometer installed at the BL-10B station of the Photon Factory in the National Laboratory for High Energy Physics (KEK).[18] With a silicon (311) channel cut monochromator, an energy resolution of 1.1 eV at 9 keV was achieved with a typical photon flux of 10^9 photons/sec, when the storage ring was operated at 2.5 GeV and 300 mA. The intensity of the incident beam, I_0, and that of the transmitted beam, I, were measured using two ionization chambers filled with 85% nitrogen-15% argon mixture for I_0 and with pure argon for I. The surveying energy region for the X-ray absorption spectra was from 12.4 keV to 13.8 keV. In a typical run it took 20 minutes to survey the energy region around Se K-edge.

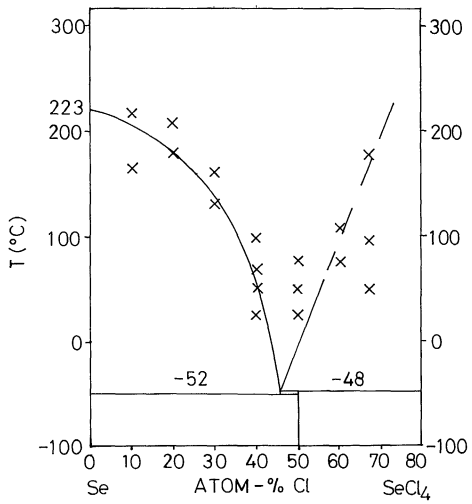

(a)

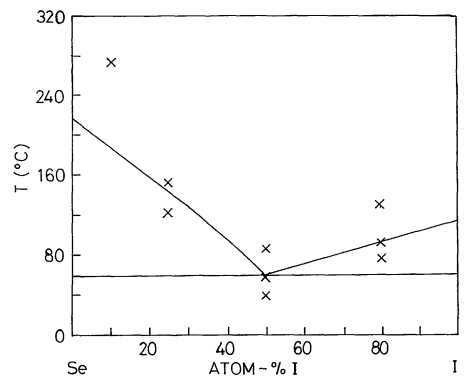

(b)

Fig. 2. The temperatures and concentrations at which EXAFS measurements were carried out are denoted by crosses on the phase diagrams of Se–Cl system[9] (a) and Se–I system[11] (b).

In order to extract the EXAFS oscillation $\chi(k)$ as a function of photoelectron wave number k, the background absorption was subtracted from the observed absorption, $\ln(I_0/I)$, using the Victreen fit in the pre-edge region. The absorption of an isolated atom $\mu_0 t$ was estimated using the cubic spline technique.[19] The subtracted spectrum was then normalized by $\mu_0 t$ to obtain $\chi(k)$.

2.3 *Pulsed neutron scattering measurements*

Pulsed neutron scattering measurements for l-$Se_{0.5}Cl_{0.5}$, l-$Se_{0.5}Br_{0.5}$ and l-$Se_{0.5}I_{0.5}$ were carried out using the HIT spectrometer[20] installed at the pulsed neutron source of KEK. HIT is a high intensity total scattering spectrometer specially designed to measure the structure factor $S(Q)$ over a wide range of momentum transfer. About ten hours were required to obtain the time-of-flight spectrum with 2048 channels for one sample, and more than ten thousand neutrons were accumulated per channel. The liquid sample was held in a cylindrical cell made of Ti–Zr null alloy; this cell had an 8.0 mm inner diameter, an 8.6 mm outer diameter, and was about 8 cm high. The measurements were carried out at room temperature for l-$Se_{0.5}Cl_{0.5}$ and l-$Se_{0.5}Br_{0.5}$, and at 75°C for l-$Se_{0.5}I_{0.5}$.

In order to extract $S(Q)$ from the measured neutron intensity, $I(Q)$, the following formula[21,22] was used to correct for absorption and multiple scattering effects:

$$S(Q)=\frac{1}{4\pi D\langle b^2\rangle}\left\{\frac{I(Q)}{A_{s,sc}}-\frac{A_{c,sc}}{A_{s,sc}A_{c,c}}I_c(Q)\right\} \div\frac{I_V(Q)}{D_V\sigma_V A_{V,V}(1+\Delta_V)}-\Delta-S_{inc}. \quad (1)$$

Here $I_c(Q)$ and $I_V(Q)$ are the measured neutron intensities for the empty Ti–Zr cell and a vanadium rod standard sample, respectively. $4\pi\langle b^2\rangle$ is the coherent scattering cross section of the sample and σ_V is the incoherent scattering cross section of vanadium. $A_{\alpha,\beta}$ is the absorption factor for neutrons which are scattered by α and transmitted by β. The subscripts c, sc, and V denote the cell, the sample plus cell, and the vanadium rod, respectively. These factors were calculated by the method proposed by Paalman and Pings.[22] Multiple scattering terms Δ for the sample plus cell and Δ_V for the vanadium rod were obtained from the work by Blech and Averbach.[23] D is the total number of atoms in the sample located in the neutron flux and D_V the number of vanadium atoms in the flux. S_{inc} is the isotropic incoherent scattering term for the sample. A more detailed description of the data processing has been given elsewhere.*

* K. Maruyama: Thesis (Kyoto University, Kyoto, 1991).

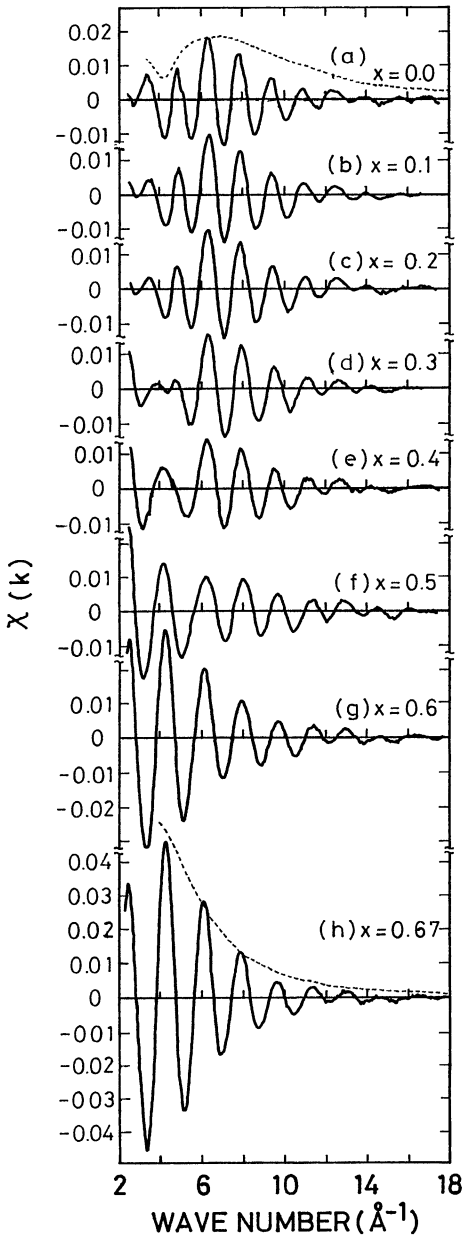

Fig. 3. The EXAFS oscillation, $\chi(k)$, near Se K-edge for l-Se at 250°C (a), l-$Se_{0.9}Cl_{0.1}$ at 220°C (b), l-$Se_{0.8}Cl_{0.2}$ at 180°C (c), l-$Se_{0.7}Cl_{0.3}$ at 130°C (d), l-$Se_{0.6}Cl_{0.4}$ at 50°C (e), l-$Se_{0.5}Cl_{0.5}$ at room temperature (f), l-$Se_{0.4}Cl_{0.6}$ at 110°C (g) and l-$Se_{0.33}Cl_{0.67}$ at 180°C (h) as a function of photoelectron wave number k. The electron backward scattering amplitudes[24] from Se and Cl atoms are shown by the broken lines in (a) and (h), respectively.

§3. Results and Discussion

3.1 EXAFS of liquid $Se_{1-x}Cl_x$

Figure 3 shows Se K-edge EXAFS oscillation, $\chi(k)$, along the liquidus curve for l-Se (a), l-$Se_{0.9}Cl_{0.1}$ (b), l-$Se_{0.8}Cl_{0.2}$ (c), l-$Se_{0.7}Cl_{0.3}$ (d), l-$Se_{0.6}Cl_{0.4}$ (e), l-$Se_{0.5}Cl_{0.5}$ (f), l-$Se_{0.4}Cl_{0.6}$ (g) and l-$Se_{0.33}Cl_{0.67}$ (h) as a function of photoelectron wave number k. The amplitude of χ(k) for l-Se exhibits a maximum around 7 A^{-1} and varies in a way similar to the backward scattering amplitude[24] from a Se atom; this is denoted by the broken line in Fig. 3(a). As the Cl concentration increases the maximum near 7 A^{-1} becomes less pronounced and the amplitude of $\chi(k)$ in low k region becomes larger. For l-$Se_{0.33}Cl_{0.67}$ the amplitude of $\chi(k)$ decreases monotonically with increasing k. This k-dependence coincides with the backward scattering amplitude[24] from a Cl atom, as denoted by the broken line in Fig. 3(h).

Figure 4 shows the radial distribution function $|F(r)|$ around Se atom for l-Se (a), l-$Se_{0.8}Cl_{0.2}$ (b), l-$Se_{0.6}Cl_{0.4}$ (c), l-$Se_{0.5}Cl_{0.5}$ (d) and l-$Se_{0.33}Cl_{0.67}$ (e). The $|F(r)|$ were obtained by a Fourier transform of $\chi(k)$:[25]

$$F(r)=\frac{1}{\sqrt{2\pi}}\int_{k_{\min}}^{k_{\max}} w(k)\,k\chi(k)\,e^{2ikr}\,dk. \quad (2)$$

We used a Hanning window for $w(k)$ to reduce the spurious peaks caused by a finite integral region. Typical values of $k_{\min}$ and $k_{\max}$ were taken to be 3.0 A^{-1} and 16 A^{-1}, respectively.

For l-Se a peak exists around 2.0 A, corresponding to the covalent bond length of Se–Se. With increasing Cl concentration the peak position shifts toward smaller r. In the concentration range above $x=0.5$, a shoulder is observed on the large r side; this may result from an interference effect between the EXAFS signals from neighboring Se and Cl atoms.

It is reasonable to assume that the Se chain is shortened by the addition of Cl, as is known from the viscosity measurements. In order to obtain the atomic arrangements of Se and Cl around a central Se atom, we carried out a curve fitting analysis. First, we calculated the back Fourier transform, $\tilde{\chi}(k)$, of $F(r)$ around the first peak. Then we fitted $k^3\tilde{\chi}(k)$ by means

of the least square method with the following EXAFS formula based on a single scattering approximation:[25]

$$k^3\tilde{\chi}(k)=S\left\{N_{Se}B_{Se}(k_{Se})k^2\exp(-2\sigma_{Se}^2k_{Se}^2)\frac{\sin(2k_{Se}r_{Se}-\phi_{Se}(k_{Se}))}{r_{Se}^2}\right.$$
$$\left.+N_{Cl}B_{Cl}(k_{Cl})k^2\exp(-2\sigma_{Cl}^2k_{Cl}^2)\frac{\sin(2k_{Cl}r_{Cl}-\phi_{Cl}(k_{Cl}))}{r_{Cl}^2}\right\}, \quad (3)$$

where

$$k_{Se}=\sqrt{k^2-0.2625\Delta E_{0Se}},$$

and

$$k_{Cl}=\sqrt{k^2-0.2625\Delta E_{0Cl}}.$$

The weighing factor k^3 was introduced to compensate for reduction of the $\tilde{\chi}(k)$ amplitude in the high k region. The first and second terms of eq. (3) represent the Se-Se and Se-Cl correlations, respectively. The subscript, Se or Cl, specifies the neighboring atom. $B_i(k)$ is the backward scattering amplitude from i-atom and $\phi_i(k)$ is the phase shift experienced by the photoelectron which is emitted from the central Se atom and scattered by neighboring i-atom. Numerical values of $B_i(k)$ and $\phi_i(k)$ are adopted from the supplement table calculated by McKale *et al.*[24] S is a scaling factor which includes the decaying effects of the photoelectron wave due to the finite mean free path. In the present analysis S was fixed to be 0.65 so as to give $N_{Se}=2$ for l-Se. N_i represents the coordination number of i-atoms which are situated at an average distance of r_i with the mean square displacement of σ_i^2. ΔE_{0i} represents a small correction to the energy of absorption edge. The values of ΔE_{0i} ranged from 4 to 7 eV. The values resulting from this fitting procedure are listed in Table I.

Figures 5(a) and 5(b) show the average coordination numbers of Se, N_{Se} and Cl, N_{Cl},

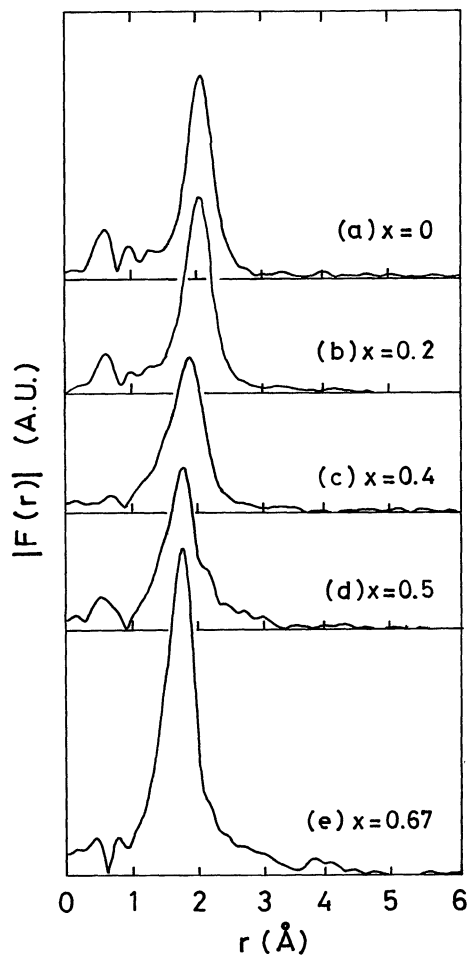

Fig. 4. The radial distribution function $|F(r)|$ around a Se atom, obtained by Fourier transform of k times $\chi(k)$, for l-Se (a), l-$Se_{0.8}Cl_{0.2}$ (b), l-$Se_{0.6}Cl_{0.4}$ (c), l-$Se_{0.5}Cl_{0.5}$ (d) and l-$Se_{0.33}Cl_{0.67}$ (e).

Table I. The coordination numbers of Se, N_{Se}, and Cl, N_{Cl}, around the central Se atom, the bond lengths of Se-Se, r_{Se}, and Se-Cl, r_{Cl}, and their root-mean-square displacements, σ_{Se} and σ_{Cl}, for l-$Se_{1-x}Cl_x$ obtained by fitting $\chi(k)$.

	Se-Se bond			Se-Cl bond		
x	N_{Se}	r_{Se}(A)	σ_{Se}(A)	N_{Cl}	r_{Cl}(A)	σ_{Cl}(A)
0.0	2.0	2.33	0.072	0.0	—	—
0.1	2.0	2.34	0.072	0.0	—	—
0.2	2.3	2.33	0.075	0.1	2.23	0.028
0.3	1.8	2.32	0.076	0.4	2.19	0.037
0.4	1.5	2.30	0.076	0.6	2.18	0.027
0.5	1.0	2.25	0.066	0.8	2.17	0.040
0.6	0.6	2.25	0.054	1.5	2.17	0.043
0.67	0.4	2.26	0.057	1.7	2.17	0.046

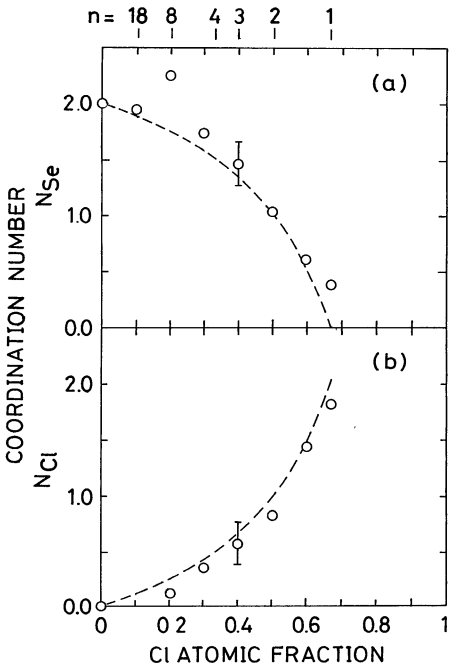

Fig. 5. The partial coordination number of Se (a) and Cl (b) around a central Se atom, derived from $\tilde{\chi}(k)$, for l-$Se_{1-x}Cl_x$, plotted as a function of x. The dashed lines are the calculated curves from eqs. (4) and (5). The numbers above the figure represent the mean chain lengths n.

around a central Se atom for l-$Se_{1-x}Cl_x$, as derived from fitting $\tilde{\chi}(k)$ with eq. (3). The temperature variation of the coordination number is very small in the measured range. The value of N_{Se} decreases with increasing Cl concentration x, being about 1 at $x=0.5$ and nearly 0 at $x=0.67$. On the other hand, N_{Cl} increases from 0 to 2 as x increases to 0.67.

Figure 6 shows schematically how the Se chain structure is modified by the addition of Cl. Since the electronegativity of Cl is much larger than that of Se, the electrons are expected to be transferred from Se to Cl when the Se chains are terminated by Cl. Here we assume that every halogen (X) atom acts as a chain terminator to form the molecules X-(-Se-)$_n$-X, where $n=2/x-2$. Then N_{Se} and N_X are given by

$$N_{Se}=\frac{2n-2}{n}=\frac{2-3x}{1-x}, \tag{4}$$

and

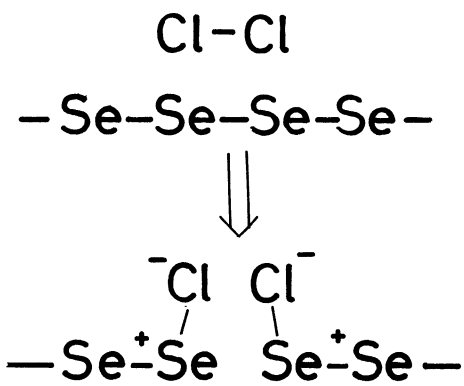

Fig. 6. A schematic illustration of how the Se chain structure is modified by the addition of Cl.

$$N_X=\frac{2}{n}=\frac{x}{1-x}. \tag{5}$$

The calculated values are shown in Fig. 5 by the dashed lines. The agreement between the observed and calculated values is good, implying that l-$Se_{1-x}Cl_x$ is composed of the molecules Cl-(-Se-)$_n$-Cl, as assumed.

Figures 7(a) and 7(b) show the bond length of Se-Se, r_{Se}, and Se-Cl, r_{Cl}, obtained from

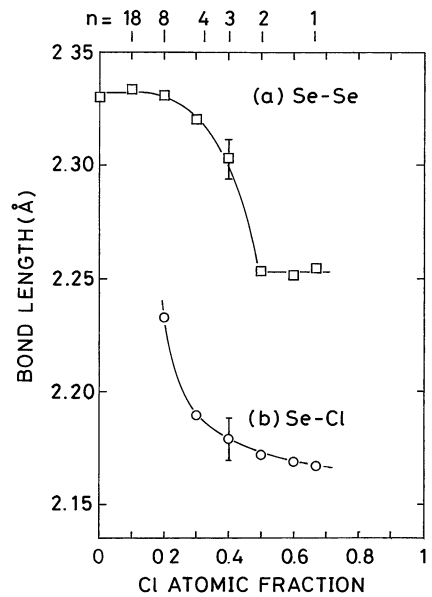

Fig. 7. The Se-Se (a) and Se-Cl (b) bond lengths, obtained from $\tilde{\chi}(k)$, plotted as a function of x for l-$Se_{1-x}Cl_x$. The solid lines are guides for the eye. The numbers above the figure represent the mean chain lengths n.

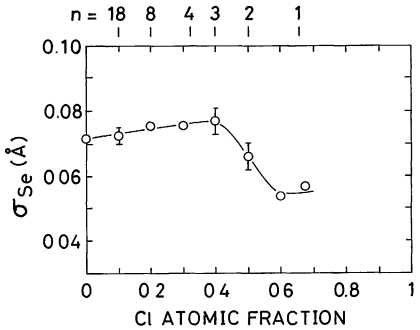

Fig. 8. Concentration variation of σ_{Se} for l-$Se_{1-x}Cl_x$. The solid line is a guide for the eye. The numbers above the figure represent the mean chain lengths n.

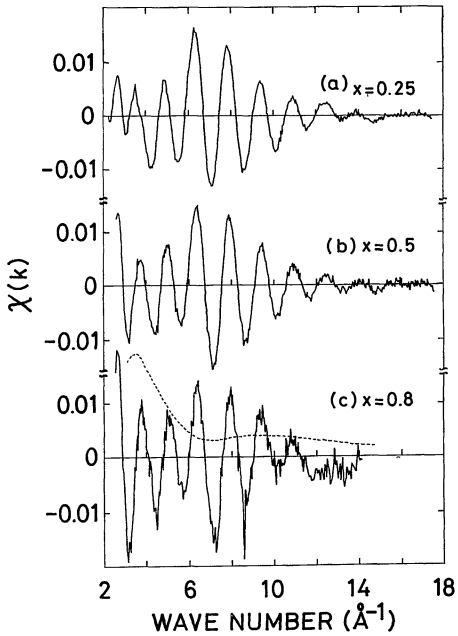

Fig. 9. The EXAFS oscillations, $\chi(k)$, near Se K-edge for l-$Se_{0.75}I_{0.25}$ at 150°C (a), l-$Se_{0.5}I_{0.5}$ at 60°C (b) and l-$Se_{0.2}I_{0.8}$ at 95°C (c) as a function of photoelectron wave number k. The electron backward scattering amplitudes[24] from I atoms is shown by the broken line in (c).

the fitting for l-$Se_{1-x}Cl_x$ as a function of x. The Se–Se bond length is nearly equal to that of pure l-Se at low x and begins to decrease near $x=0.2$, where n is estimated to be 8. A sharp drop is seen when x approaches to 0.5, where most molecules are expected to have a structural formula Cl–Se–Se–Cl. For $x \geqq 0.5$, the Se–Se bond length is independent of x. The charge transfer from Se to Cl leaves a hole in the lonepair orbital of Se and an additional π-bond tends to be formed between Se atoms. This may result in the contraction of the Se–Se bond. A rapid contraction of the Se–Cl bond is also observed when x increases to 0.5. The Se–Cl bond length above $x=0.5$ is comparable to the sum of covalent radii of Se and Cl.

The Cl impurity is considered to act as a charged additive. However, the experimental evidence that Se–Cl bonds contract with decreasing n may suggest that the bonding nature between Se and Cl changes from ionic to covalent. As shown in Fig. 8, σ_{Se} decreases rapidly near $x=0.5$, which implies that fluctuations in the bond length are small for the simple molecules.

3.2 *EXAFS of liquid $Se_{1-x}I_x$*

Figure 9 shows Se K-edge EXAFS oscillations, $\chi(k)$, along the liquidus curve for l-$Se_{0.75}I_{0.25}$ (a), l-$Se_{0.5}I_{0.5}$ (b) and l-$Se_{0.2}I_{0.8}$ (c) as a function of photoelectron wave number k. For l-$Se_{1-x}I_x$, amplitude of $\chi(k)$ in low k region becomes larger when the I concentration increases. The backward scattering amplitude[24] from I atom is shown in Fig. 9(c) by the broken line. It is observed that the maximum in the amplitude of $\chi(k)$ at around $k=7$ A^{-1} still exists for $x=0.8$, suggesting that the Se–Se bond persists at high I concentrations in the Se–I system.

Figure 10 shows the radial distribution function $|F(r)|$ around Se atom for l-$Se_{0.75}I_{0.25}$ (a), l-$Se_{0.5}I_{0.5}$ (b) and l-$Se_{0.2}I_{0.8}$ (c); this was obtained by a Fourier transform of k times $\chi(k)$. The peak position shifts slightly towards larger r and the peak becomes broader with increasing I concentration.

The $\chi(k)$ spectra for l-$Se_{1-x}I_x$ were fitted with the same method as for l-$Se_{1-x}Cl_x$ to get the structural parameters. Table II shows the resulting values. Figures 11(a) and 11(b) display the coordination numbers of Se, N_{Se}, and I, N_I, around a central Se atom for l-$Se_{1-x}I_x$ as a function of x. With increasing x, N_{Se} decreases and N_I increases. The dashed line in Fig. 11 represents the concentration variation of N_{Se} and N_X described by eqs. (4) and (5). The N_I curve deviates downwards from what it would be if all I atoms were chain terminators,

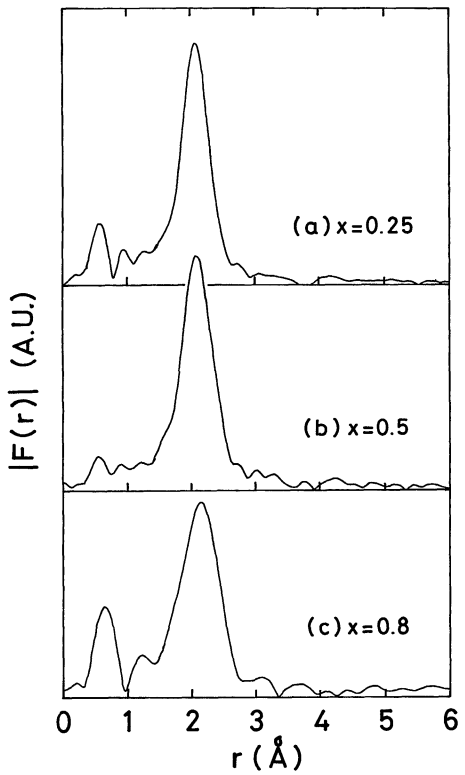

Fig. 10. The radial distribution function $|F(r)|$ around a central Se atom, obtained from Fourier transform of k times $\chi(k)$, for l-$Se_{0.75}I_{0.25}$ (a), l-$Se_{0.5}I_{0.5}$ (b) and l-$Se_{0.2}I_{0.8}$ (c).

Table II. The coordination numbers of Se, N_{Se}, and I, N_I, around the central Se atom, the bond lengths of Se–Se, r_{Se}, and Se–I, r_I, and their root-mean-square displacements, σ_{Se} and σ_I, for l-$Se_{1-x}I_x$ obtained by fitting $\chi(k)$.

	Se–Se bond			Se–I bond		
x	N_{Se}	r_{Se}(A)	σ_{Se}(A)	N_I	r_I(A)	σ_I(A)
0.1	2.0	2.34	0.072	0.0	—	—
0.25	1.7	2.34	0.063	0.2	2.55	0.048
0.5	1.5	2.33	0.058	0.4	2.56	0.053
0.8	1.1	2.31	0.036	0.5	2.56	0.028

and the N_{Se} does not tend to zero even for high x. Therefore I atoms are not always incorporated into the chain molecules, in contrast to Cl atoms. The excess I atoms may form I_2 molecules. Figures 12(a) and 12(b) show the Se–Se and Se–I bond length for l-$Se_{1-x}I_x$ as a function of x. The Se–Se bond length becomes slightly shorter with increasing x and Se–I bond changes little. This suggests that the charge transfer between Se and I atoms is small. The strength of the I–Se bond is nearly equal to that of the I–I bond; hence they may be interchangeable as shown in Fig. 13.

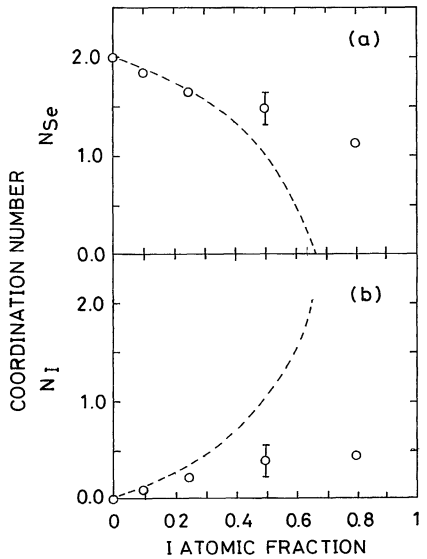

Fig. 11. The partial coordination numbers of Se (a) and I (b) around a central Se atom, derived from $\tilde{\chi}(k)$, for l-$Se_{1-x}I_x$ and plotted as a function of x. The dashed lines are the calculated curves from eqs. (4) and (5).

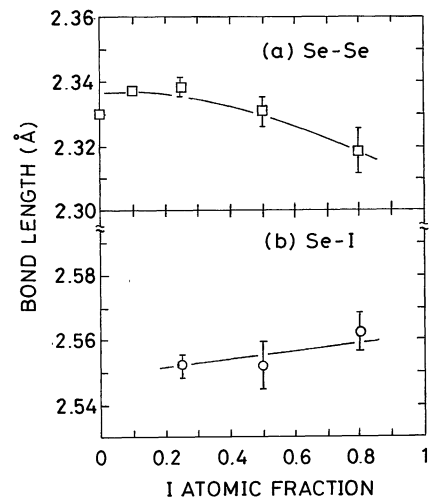

Fig. 12. The Se–Se (a) and Se–I (b) bond lengths for l-$Se_{1-x}I_x$, derived from $\tilde{\chi}(k)$, plotted as a function of x. The solid lines are guides for the eye.

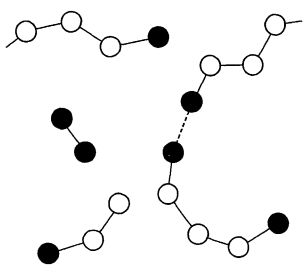

Fig. 13. Illustration of an expected structure of a liquid Se–I mixture. The open and closed circles represent Se and I atoms, respectively.

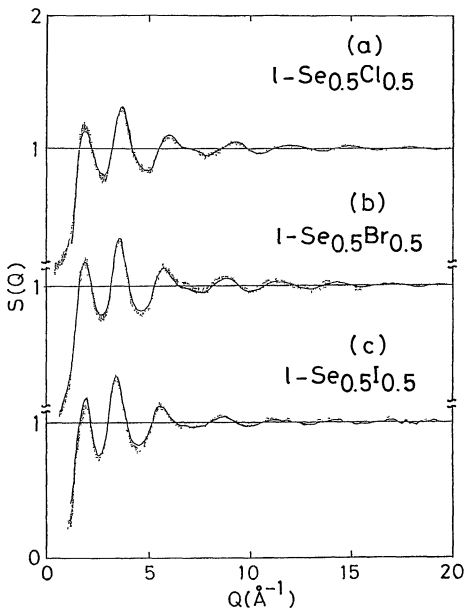

Fig. 14. The structure factor $S(Q)$ deduced from the pulsed neutron scattering measurement for l-$Se_{0.5}Cl_{0.5}$ (a), l-$Se_{0.5}Br_{0.5}$ (b) and l-$Se_{0.5}I_{0.5}$ (c). The solid lines are the Fourier transforms of total pair distribution function $g(r)$ in the r range above 2.0 A.

3.3 *Structure factor of l-$Se_{0.5}Cl_{0.5}$, l-$Se_{0.5}Br_{0.5}$ and l-$Se_{0.5}I_{0.5}$*

Figure 14 shows the total structure factor $S(Q)$ obtained by neutron scattering measure-

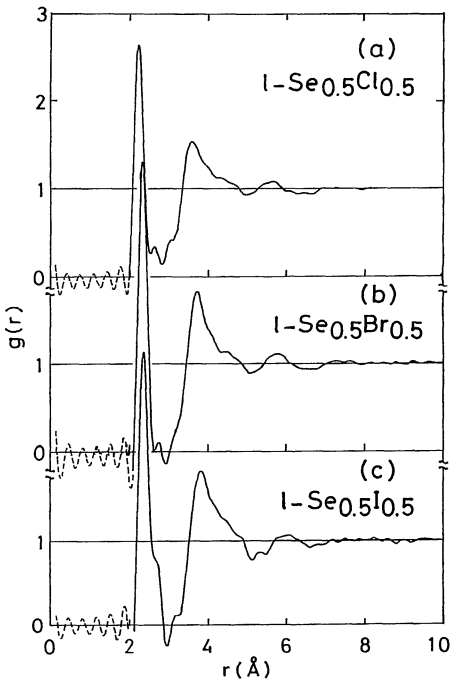

Fig. 15. The total pair correlation function $g(r)$, derived by Fourier transform of $S(Q)$, for l-$Se_{0.5}Cl_{0.5}$ (a), l-$Se_{0.5}Br_{0.5}$ (b) and l-$Se_{0.5}I_{0.5}$ (c).

ments for l-$Se_{0.5}Cl_{0.5}$ at room temperature (a), l-$Se_{0.5}Br_{0.5}$ at room temperature (b) and l-$Se_{0.5}I_{0.5}$ at 75°C (c). The dots represent the experimental data and the solid lines the back Fourier transform of the total pair correlation function $g(r)$.

For l-$Se_{0.5}Cl_{0.5}$, the first peak appears at around 2.0 A^{-1}. The second peak, at about 3.5 A^{-1}, is higher than the first, and the third peak has a shoulder on the high Q side. Oscillations in $S(Q)$ are seen clearly even in the high Q region near 15 A^{-1}. For l-$Se_{0.5}Br_{0.5}$ and l-$Se_{0.5}I_{0.5}$, $S(Q)$ is similar to that of l-$Se_{0.5}Cl_{0.5}$ except that the shoulder on the third peak is blurred.

Figure 15 shows $g(r)$ of l-$Se_{0.5}Cl_{0.5}$ (a), l-$Se_{0.5}Br_{0.5}$ (b) and l-$Se_{0.5}I_{0.5}$ (c) derived from eq. (6):

$$g(r)=1+\frac{1}{8\pi^3 n_0}\int_0^{Q_{max}}\{S(Q)-1\}\frac{\sin(Qr)}{Qr}4\pi Q^2 w(Q)\,dQ, \tag{6}$$

where n_0 denotes the number density of atoms and $w(Q)$ is the Hanning window function. A sharp and distinct first peak is seen around $r=2.2$ A for l-$Se_{0.5}Cl_{0.5}$. This peak may correspond to

the Se–Se and Se–Cl bonds within the Cl–Se–Se–Cl molecule. The second peak of $g(r)$ has a rather asymmetric shape, with a tail extending on the large r side. The $g(r)$ curve is severely damped at distances longer than 7 A; this feature is consistent with the EXAFS result that no long chain molecule exists.

The shape of $g(r)$ for l-$Se_{0.5}Br_{0.5}$ is nearly the same as for l-$Se_{0.5}Cl_{0.5}$, although the first peak shifts to larger r and its width is narrower. For l-$Se_{0.5}I_{0.5}$, $g(r)$ has a shoulder on the high-r side of the first peak.

From the EXAFS results it was found that l-$Se_{0.5}Cl_{0.5}$ is composed mainly of Cl–Se–Se–Cl molecules. As a first step, we deduced the intramolecular structure factor $F_1(Q)$ from the observed $S(Q)$ in high Q range, where the intermolecular structure factor is expected to be reduced substantially. The $S(Q)$ data were analyzed in the Q range from 10 to 19 A^{-1} by using the following equation:

$$F_1(Q)=1+\frac{1}{b_{Se}^2+b_{Cl}^2}\left\{b_{Se}^2\frac{\sin(QR_{SeSe})}{QR_{SeSe}}\exp\left(-\frac{Q^2\sigma_{SeSe}^2}{2}\right)+b_{Cl}^2\frac{\sin(QR_{ClCl})}{QR_{ClCl}}\exp\left(-\frac{Q^2\sigma_{ClCl}^2}{2}\right)\right.$$
$$\left.+2b_{Se}b_{Cl}\left[\frac{\sin(QR_{SeCl(1)})}{QR_{SeCl(1)}}\exp\left(-\frac{Q^2\sigma_{SeCl(1)}^2}{2}\right)+\frac{\sin(QR_{SeCl(2)})}{QR_{SeCl(2)}}\exp\left(-\frac{Q^2\sigma_{SeCl(2)}^2}{2}\right)\right]\right\}, \quad (7)$$

where b_{Se} and b_{Cl} are the coherent scattering length of the Se and Cl nuclei, respectively. $R_{\alpha\beta}$ is an atomic distance between α and β atoms and $\sigma_{\alpha\beta}$ is its root-mean-square displacement. The subscripts SeSe and ClCl indicate the intramolecular Se–Se and Cl–Cl atom pairs. SeCl(1) indicates the directly bonded Se–Cl pair and SeCl(2) is the second neighboring Se–Cl pair.

The agreement between the calculated $F_1(Q)$ and observed $S(Q)$ curve was excellent in the Q range $7<Q<20$ A^{-1}, which is much wider than the fitting range. This confirms the existence of Cl–Se–Se–Cl molecule in l-$Se_{0.5}Cl_{0.5}$. The same analysis was carried out for l-$Se_{0.5}Br_{0.5}$ and l-$Se_{0.5}I_{0.5}$. In Table III, the atomic distances and their root-mean-square displacements, the bond angle formed between the Se–Se and the Se–halogen (X) pairs, and the dihedral angle are listed for l-$Se_{0.5}Cl_{0.5}$, l-$Se_{0.5}Br_{0.5}$ and l-$Se_{0.5}I_{0.5}$. The Se–Se and Se–X bond length in l-$Se_{0.5}Cl_{0.5}$ and l-$Se_{0.5}I_{0.5}$ obtained from neutron scattering are in fairly good agreement with the EXAFS results. However, the shoulder on the first peak of $g(r)$ for l-$Se_{0.5}I_{0.5}$ could not be reproduced by the above analysis.

As an alternative, the first peak of $g(r)$ was fitted on the assumption that the liquid is composed by I–(–Se–)$_n$–I and I_2 molecules. The results indicated that the shoulder of the first peak could be assigned to the I–I bond length of 2.7 A in the I_2 molecule, and that n was about 3.

Next, we considered the intermolecular correlation of Cl–Se–Se–Cl molecules in liquid state. Recently Misawa,[26-28] extending an idea by Egelstaff *et al.*,[29] has proposed a new realistic method for deducing orientational correlation from the measured total structure factor. In this method $S(Q)$ is written as:

$$S(Q)=S_u(Q)+\Delta S(Q), \quad (8)$$

Table III. The atomic distances and their root-mean-square displacements, the bond angle formed between the Se–Se and the Se-halogen (X) bonds, and the dihedral angle for the X–Se–Se–X molecule (X=Cl, Br and I), obtained by fitting $S(Q)$ in the Q region from 10 to 19 A^{-1}.

Sample	Atomic distances/root-mean-square displacement Se–Se	Se–X(1)	Se–X(2)	X–X
l-$Se_{0.5}Cl_{0.5}$	2.32 A ±0.06	2.19 A ±0.08	3.52 A ±0.14	4.37 A ±0.20
l-$Se_{0.5}Br_{0.5}$	2.28 ±0.07	2.38 ±0.09	3.66 ±0.14	4.57 ±0.18
l-$Se_{0.5}I_{0.5}$	2.34 ±0.08	2.52 ±0.19	3.75 ±0.16	4.77 ±0.19

Sample	Bond angle	Dihedral angle
l-$Se_{0.5}Cl_{0.5}$	102°	85°
l-$Se_{0.5}Br_{0.5}$	104	83
l-$Se_{0.5}I_{0.5}$	101	89

where $S_u(Q)$ is the structure factor of the liquid consisting of completely uncorrelated molecules and $\Delta S(Q)$ is a correlation term arising from preferred orientation. Using the intramolecular structure factor $F_1(Q)$, $S_u(Q)$ is given by:[29]

$$S_u(Q)=F_1(Q)+F_u(Q)\{S_{hs}(Q)-1\}\exp(-\Delta_{hs}^2 Q^2/2). \tag{9}$$

Here $F_u(Q)$ is known as the intermolecular form factor, which was first derived by Zachariasen[30] and is expressed in this case as

$$F_u(Q)=\frac{2}{b_{Se}^2+b_{Cl}^2}\left\{b_{Se}\frac{\sin(Qr_{Se})}{Qr_{Se}}+b_{Cl}\frac{\sin(Qr_{Cl})}{Qr_{Cl}}\right\}^2. \tag{10}$$

In eq. (10), r_{Se} and r_{Cl} denote distances of Se and Cl atoms from the center of Se–Se bond. The value of r_{Se} and r_{Cl} are determined from the molecular structure listed in Table III. The structure factor of the center of Se–Se bond, $S_{hs}(Q)$, is assumed to be given by the Percus-Yevick hard-sphere model, having an effective diameter s.[31] Δ_{hs} is the damping factor introduced to minimize the oscillation in the high Q region caused by the hard sphere potential.

We assumed further that the Se–Se bond in a molecule is parallel to that in neighboring molecules, as seen in crystalline phase,[12] in order to reduce the number of the fitting parameters. Thus the orientational correlation is given by the spherical coordinates (R_c, θ, ϕ) of the center of Se–Se bond in the second molecule relative to the center of first molecule, and the molecular rotation Θ around the Se–Se bond of the second molecule. (See Fig. 16). The correlation term $\Delta S(Q)$ is given by:

$$\Delta S(Q)=n_c\left\{\frac{1}{2b_{Se}^2+2b_{Cl}^2}\sum_{ij}b_i b_j\frac{\sin(QR_{ij})}{QR_{ij}}\exp\left(-\frac{\sigma_{ij}^2Q^2}{2}\right)\right.$$
$$\left.-F_u(Q)\frac{\sin(QR_u)}{QR_u}\exp\left(-\frac{\Delta R_u^2Q^2}{2}\right)\right\}. \tag{11}$$

where R_{ij} is the distance between two atoms in different molecules and is a function of R_c, θ, ϕ and Θ. σ_{ij} is the root-mean-square displacement of R_{ij}, and for simplicity is assumed to

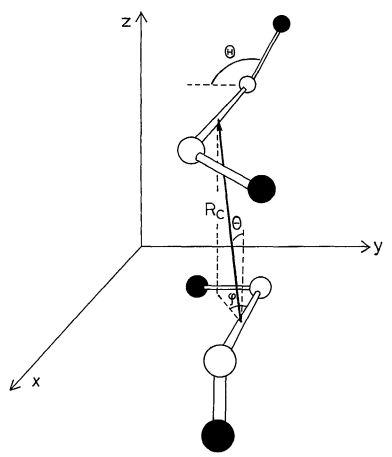

Fig. 16. Definition of parameters for the spherical coordination (R_c, θ, ϕ) relative to the center of Se–Se bond and the molecular rotation Θ. The most probable orientation of two Cl–Se–Se–Cl molecules is indicated schematically.

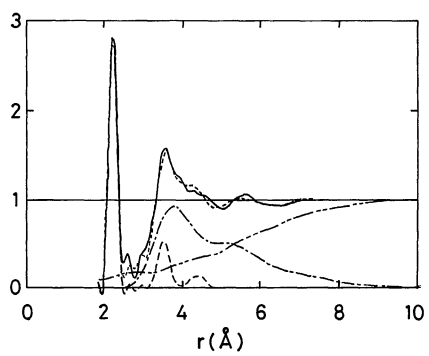

Fig. 17. A comparison of the measured and calculated pair correlation function, $g(r)$, for l-$Se_{0.5}Cl_{0.5}$. The solid line shows the observed $g(r)$ and dotted line the calculated one. The dot-dashed line denotes the correlation between the orientationally correlated neighboring molecules, and the dot-dot-dashed line the intermolecular distribution without orientational correlation.

Table IV. The intermolecular configuration parameters obtained by fitting the $S(Q)$ for l-$Se_{0.5}Cl_{0.5}$ and l-$Se_{0.5}Br_{0.5}$.

Sample	R_c	θ	ϕ	Θ	n_c	δ_c	s	Δ_{hs}	R_u	ΔR_u
l-$Se_{0.5}Cl_{0.5}$	4.2 A	35°	50°	53°	5.9	0.10	3.9 A	0.03 A	4.9 A	0.1 A
l-$Se_{0.5}Br_{0.5}$	4.5	38	50	52	6.4	0.08	4.2	0.02	4.7	0.3

be proportional to the atomic spacing, i.e. $\sigma_{ij} = \delta_c R_{ij}$. The subtraction of the second term on the right hand side of eq. (11) is needed to replace the uncorrelated nearest neighboring molecules by the correlated ones. R_u is what the distance between the centers of the two molecules would be if they were in an uncorrelated orientation. n_c is the number of correlated molecules.

The most probable orientation was determined by fitting of the observed $S(Q)$ with eqs. (9) and (11). The fitting parameters were n_c, θ, ϕ, Θ, R_c, δ_c, s, Δ_{hs}, R_u and ΔR_u. Since Cl-Se-Se-Cl is a chiral molecule, there are two configurations of molecular pair. The fitting was better for the antipodal configuration. In Fig. 17 the calculated $g(r)$ (dotted line) is compared with the observed one (solid line). The dot-dashed line denotes the correlation between the orientationally correlated neighboring molecules and the dot-dot-dashed line indicates the intermolecular distribution without orientational correlation. The dashed line represents the intramolecular distribution. The first peak of $g(r)$ is composed fully of intramolecular Se-Se and Se-Cl bonds, and the asymmetric second peak near 3.6 A is mainly a result of intermolecular Se-Cl correlations. The probable orientational correlation between neighboring molecules is illustrated schematically in Fig. 16.

The same analysis was carried out for l-$Se_{0.5}Br_{0.5}$, and the intermolecular structural parameters are listed in Table IV for both l-$Se_{0.5}Cl_{0.5}$ and l-$Se_{0.5}Br_{0.5}$.

§4. Summary

We have studied the structure of liquid selenium-halogen mixtures via EXAFS and neutron scattering measurements. From the EXAFS measurements, the concentration variation of the coordination numbers of Se and halogen atoms around the central Se atom were determined. The results reveal that all Cl atoms in l-$Se_{1-x}Cl_x$ act as chain terminators. The rapid contraction of Se-Se and Se-Cl bonds is observed when the Cl concentration approaches to 0.5, where most molecules have a structural formula Cl-Se-Se-Cl. For l-$Se_{1-x}I_x$, I atoms are not always incorporated in the chain molecules and the excess I atoms form I_2 molecules. This suggests that the charge transfer between Se and I is small and that the I-Se and I-I bonds are interchangeable.

Both the intra- and the intermolecular structures were obtained for l-$Se_{0.5}Cl_{0.5}$ and l-$Se_{0.5}Br_{0.5}$ from neutron scattering measurements. The first peak of $g(r)$ is fully composed of intramolecular Se-Se and Se-X bonds, and the asymmetric second peak is mainly a result of intermolecular Se-X correlations.

Acknowledgment

The authors are grateful to Drs. M. Inui and Y. Katayama, Professors K. Tamura and H. Hoshino, Dr. S. Hosokawa and Mr. T. Tsuzuki for their technical assistance.

References

1) J. C. Perron, J. Rabit and J. F. Rialland: Philos. Mag. **46** (1982) 321.
2) W. Freyland and M. Cutler: J. Chem. Soc. Faraday II **76** (1980) 750.
3) M. Misonou and H. Endo: Ber. Bunsenges. Phys. Chem. **86** (1982) 645.
4) W. W. Warren, Jr. and R. Dupree: Phys. Rev. **B22** (1980) 2257.
5) M. Misonou and H. Endo: J. Phys. Soc. Jpn. **51** (1982) 2285.
6) T. Shirai, S. Hamada and K. Kobayashi: Nippon Kagaku Zasshi **84** (1963) 968 [in Japanese].
7) M. Yao, S. Hosokawa and H. Endo: J. Non-Cryst. Solids **59&60** (1983) 1083.
8) S. Hosokawa, M. Yao, T. Yoshimura and H. Endo: J. Phys. Soc. Jpn. **54** (1985) 4717.
9) P. Born, R. Kniep, D. Mootz, M. Hein and B. Krebs: Z. Naturforsch. **36b** (1981) 1516.
10) P. Born, R. Kniep and D. Mootz: Z. Anorg. Allg. Chem. **451** (1979) 12.

11) S. N. Chzhevskaya, N. Kh. Abrikosov and B. R. Azizowa: Izv. Akad. Nauk SSSR, Neorg. Mater. **9** (1973) 218.
12) R. Kniep, L. Korte and D. Mootz: Z. Naturforsch. **38b** (1983) 1.
13) M. Lundkvist: Acta Chem. Scand. **22** (1968) 281.
14) M. Lundkvist and M. Lellep: Acta Chem. Scand. **22** (1968) 291.
15) D. M. Yost and C. E. Kircher: J. Am. Chem. Soc. **52** (1930) 4680.
16) K. Tamura, M. Inui, H. Endo, S. Hosokawa, H. Hoshino, Y. Katayama and K. Maruyama: J. Phys.: Condens. Matter. in press.
17) E. D. Crozier, F. W. Lytle, D. E. Sayers and A. Stern: Can. J. Chem. **55** (1977) 1968.
18) M. Nomura and A. Koyama: KEK Report **89-16** (1989).
19) M. Inui, M. Yao and H. Endo: J. Phys. Soc. Jpn. **57** (1988) 553.
20) Y. Ishikawa: Physica **120B** (1983) 3.
21) K. Suzuki, M. Misawa, K. Kai and N. Watanabe: Nucl. Instrum. Methods **147** (1977) 519.
22) H. H. Paalman and C. J. Pings: J. Appl. Phys. **33** (1962) 2635.
23) I. A. Blech and B. L. Averbach: Phys. Rev. **137** (1965) 1113.
24) A. G. McKale, B. W. Veal, A. P. Paulikas, S.-K. Chan and G. S. Knapp: J. Am. Chem. Soc. **111** (1988) 3763.
25) B. K. Teo: EXAFS: *Basic Principles and Data Analysis* (Springer-Verlag, Berlin, 1986) Chap. 4.
26) M. Misawa: J. Chem. Phys. **90** (1989) 6563.
27) M. Misawa: J. Chem. Phys. **91** (1989) 2575.
28) M. Misawa: J. Chem. Phys. **91** (1989) 5648.
29) P. A. Egelstaff, D. I. Page and J. G. Powls: Mol. Phys. **20** (1971) 881.
30) W. H. Zachariasen: Phys. Rev. **47** (1935) 277.
31) N. W. Ashcroft and J. Lekner: Phys. Rev. **145** (1966) 83.